PHOTONICS Research

Quantum non-demolition measurement based on an SU(1,1)-SU(2)-concatenated atom-light hybrid interferometer

GAO-FENG JIAO,[1] KEYE ZHANG,[1] L. Q. CHEN,[1,5] CHUN-HUA YUAN,[1,*] AND WEIPING ZHANG[2,3,4]

[1]State Key Laboratory of Precision Spectroscopy, Quantum Institute for Light and Atoms, Department of Physics, East China Normal University, Shanghai 200062, China
[2]School of Physics and Astronomy, and Tsung-Dao Lee Institute, Shanghai Jiao Tong University, Shanghai 200240, China
[3]Shanghai Research Center for Quantum Sciences, Shanghai 201315, China
[4]Collaborative Innovation Center of Extreme Optics, Shanxi University, Taiyuan 030006, China
[5]e-mail: lqchen@phy.ecnu.edu.cn
*Corresponding author: chyuan@phy.ecnu.edu.cn

Received 14 October 2021; revised 25 November 2021; accepted 27 November 2021; posted 30 November 2021 (Doc. ID 445858); published 28 January 2022

Quantum non-demolition (QND) measurement is an important tool in the fields of quantum information processing and quantum optics. The atom-light hybrid interferometer is of great interest due to its combination of an atomic spin wave and an optical wave, which can be utilized for photon number QND measurement via the AC-Stark effect. In this paper, we present an SU(1,1)-SU(2)-concatenated atom-light hybrid interferometer, and theoretically study QND measurement of the photon number. Compared to the traditional SU(2) interferometer, the signal-to-noise ratio in a balanced case is improved by a gain factor of the nonlinear Raman process (NRP) in this proposed interferometer. Furthermore, the condition of high-quality QND measurement is analyzed. In the presence of losses, the measurement quality is reduced. We can adjust the gain parameter of the NRP in the readout stage to reduce the impact due to losses. Moreover, this scheme is a multiarm interferometer, which has the potential of multiparameter estimation with many important applications in the detection of vector fields, quantum imaging, and so on.

https://doi.org/10.1364/PRJ.445858

1. INTRODUCTION

Quantum measurement takes place at the interface between the quantum world and macroscopic reality. According to quantum mechanics, as soon as we observe a system, we actually perturb it, and such perturbation cannot be reduced to zero; instead, there is a fundamental limit given by the Heisenberg uncertainty relation. Quantum non-demolition (QND) is motivated to get as close as possible to this limit [1–3]. In QND measurement, a signal observable of the measured system is coupled to a readout observable of a probe system through an interaction, so that the information about the measured quantity can be obtained indirectly by the direct measurement of the readout observable. The key issue is to design the measurement scheme in which the back action noise is transferred to the other unmeasured conjugate observable without being coupled back to the quantity of interest. The QND measurement was studied in a variety of quantum systems, including mechanical oscillators [4,5], trapped ions [6,7], solid-state spin qubits [8,9], circuit quantum electrodynamics [10,11], and photons [12–14].

In the quantum optics community, Imoto *et al.* [15] proposed an optical interferometer for a QND measurement scheme of the photon number using the optical Kerr effect, in which the cross-Kerr interaction encodes the photon number of the signal state onto a phase shift of the probe state. Subsequently, some works on photon number QND measurement were studied [16–21]. However, the main obstacles to optical QND measurement using cross-phase modulation based on third-order nonlinear susceptibilities $\chi^{(3)}$ are the small values of nonlinearity in the available media and the absorption of photons. Munro *et al.* [22] presented an implementation of the QND measurement scheme with the required nonlinearity provided by the giant Kerr effect achievable with AC-Stark electromagnetic transparency. In addition, schemes using cavity or circuit quantum electrodynamical systems have enabled photon number QND measurements that do not rely on the material nonlinearity through strong light–matter interactions [23–27].

Interferometric measurements allow for highly sensitive detection of any small changes that induce an optical phase shift.

Different kinds of quantum interferometers have been proposed for phase measurement [28–37]. The phase sensitivity of the SU(2) interferometer with coherent state input, such as the Michelson or Mach–Zehnder interferometer, is limited by the shot noise limit. When the unused port of the interferometer is fed with a squeezed state, the SU(2) interferometer can beat this limit [28]. In contrast to the SU(2) interferometer, the SU(1,1) nonlinear interferometer, which replaces the beam splitters in the SU(2) interferometer with nonlinear gain media, is a fundamentally different type of interferometric detector [29], in which quantum correlations are generated within the interferometer, and the phase sensitivity can, in principle, approach the Heisenberg limit.

Recently, using the coherent mixing of an optical wave and an atomic spin wave, the atom-light hybrid interferometer has been proposed and studied [38–44]. Similarly, there are two types of atom-light hybrid interferometers, which have also been demonstrated experimentally. One is an SU(2)-type atom-light hybrid interferometer [40], where the linear Raman processes (LRPs) replace the beam splitters in the SU(2) linear interferometer to realize linear superposition of the atomic wave and optical wave. The other is an SU(1,1)-type atom-light hybrid interferometer [41], where the nonlinear Raman processes (NRPs) realize the atomic wave and optical wave splitting and recombination. The atom-light hybrid interferometer has drawn considerable interest because it is sensitive to both optical and atomic phase shifts. Resorting to an AC-Stark effect for the atomic phase change, the atom-light hybrid interferometer can be applied to QND measurement of photon numbers [45,46]. Further developing methods to improve measurement procision is always desired for the innovation of interferometers.

In this paper, we present an SU(1,1)-SU(2)-concatenated atom-light hybrid interferometer, which is a combination of SU(2)- and SU(1,1)-type atom-light hybrid interferometers. The AC-Stark effect encodes the photon number of the signal light onto a phase shift of the atomic spin wave, so that the problem of detecting photon numbers is translated into the problem of detecting the atomic phase shift. Thus we theoretically analyze the SNR of the interferometer for precision measurement of the phase shift to examine the performance of this scheme as a QND measurement. An ideal QND measurement can be verified by a perfect correlation between the signal light and the probe system [47]. Here we estimate the quality of QND measurement using the criteria in Ref. [47], and the condition for a perfect correlation is given. In the presence of losses, the measurement quality is reduced. However, we can adjust the gain parameter of the NRP in the readout stage to reduce the impact due to losses.

Our scheme can be thought of as inserting an SU(2)-type atom-light hybrid interferometer into one of the arms of the SU (1,1)-type atom-light hybrid interferometer. Compared to a conventional SU(1,1) interferometer, the number of phase-sensing particles is further increased due to input field $\hat{a}_W^{(0)}$. In the previous scheme [45], a strong stimulated Raman process could indeed be used to excite most of the atoms to the $|m\rangle$ state to improve the number of phase-sensing particles. However, this will produce additional nonlinear effects and noise light fields [48–50]. Therefore, in the current scheme, first a spontaneous Raman process is used, and then an LRP is used to generate the Rabi-like superposition oscillation between light and the atom. By controlling the interaction time, more atoms can be prepared to the $|m\rangle$ state to improve the number of phase-sensing particles and thus to enhance the QND measurement. Compared to previous works [45,46], the SU(1,1)-SU(2)-concatenated atom-light hybrid interferometer can realize QND measurement of photon numbers with higher precision. Since the SU(2)-type and SU(1,1)-type atom-light hybrid interferometers [40,41] have been demonstrated experimentally, the SU(1,1)-SU(2)-concatenated atom-light hybrid interferometer can be realized with current experimental conditions, and the corresponding experimental requirements are given in the Discussion section.

2. SU(1,1)-SU(2)-CONCATENATED ATOM–LIGHT HYBRID INTERFEROMETER

An SU(1,1)-SU(2)-concatenated atom-light hybrid interferometer is shown in Fig. 1(a). The corresponding energy levels of the atom and optical frequencies for the formation of the SU(1,1)-SU(2)-concatenated atom-light hybrid interferometer are given in Fig. 1(b), where the lower two energy states $|g\rangle$ and $|m\rangle$ are the hyperfine split ground states. The higher-energy state $|e\rangle$ is the excited state. The strong pump field $A_{p_1}(A_{p_2})$ and strong read field $E_{p_1}(E_{p_2})$ couple transitions $|g\rangle \to |e\rangle$ and $|m\rangle \to |e\rangle$, respectively. The process can be used to describe the linear and nonlinear splitting and recombination of the light field and spin wave, i.e., NRP and LRP.

In the case of undepleted read field approximation, the two-mode coupled Hamiltonian is written as [40]

$$\hat{H}_{\mathrm{LRP}} = i\hbar\Omega\hat{a}_W\hat{S}_a^\dagger + \mathrm{H.c.}, \tag{1}$$

where $\hat{S}_a \equiv (1/\sqrt{N})\sum_k |g\rangle_{kk}\langle m|$ is the spin wave (atomic collective excitation), with N the number of atoms in the ensemble, and Ω is the Rabi-like frequency. The Rabi-like oscillation between the write field and the atomic spin wave occurs, and the input–output relation is given by

$$\begin{aligned}\hat{S}_a^{(\mathrm{out})} &= \hat{S}_a^{(\mathrm{in})}\cos(|\Omega|\tau_r) - \hat{a}_W^{(\mathrm{in})}\sin(|\Omega|\tau_r),\\ \hat{a}_W^{(\mathrm{out})} &= \hat{a}_W^{(\mathrm{in})}\cos(|\Omega|\tau_r) + \hat{S}_a^{(\mathrm{in})}\sin(|\Omega|\tau_r),\end{aligned} \tag{2}$$

where τ_r is the interaction time of read field E_p. This transform of Eq. (2) can be used for LRP. In the case of undepleted pump field approximation, the Hamiltonian is written as [41]

$$\hat{H}_{\mathrm{NRP}} = i\hbar\eta A_p\hat{a}_S^\dagger\hat{S}_a^\dagger + \mathrm{H.c.}, \tag{3}$$

where η is the coupling coefficient, and A_p is the amplitude of the pump beam. The input–output relation is given by

$$\hat{S}_a^{(\mathrm{out})} = G\hat{S}_a^{(\mathrm{in})} + ge^{i\theta}\hat{a}_S^{\dagger(\mathrm{in})}, \quad \hat{a}_S^{(\mathrm{out})} = G\hat{a}_S^{(\mathrm{in})} + ge^{i\theta}\hat{S}_a^{\dagger(\mathrm{in})}, \tag{4}$$

where $e^{i\theta} = \eta A_p/|\eta A_p|$, $G = \cosh(|\eta A_p|\tau_p)$, and $g = \sinh(|\eta A_p|\tau_p)$ are the gains of the process, with $G^2 - g^2 = 1$, τ_p the pulse duration of pump beam A_p. This transform of Eq. (4) can be used for NRP.

Next, according to the above linear and nonlinear transforms, the output operators of the SU(1,1)-SU(2)-concatenated atom-light hybrid interferometer are worked out as a function of the

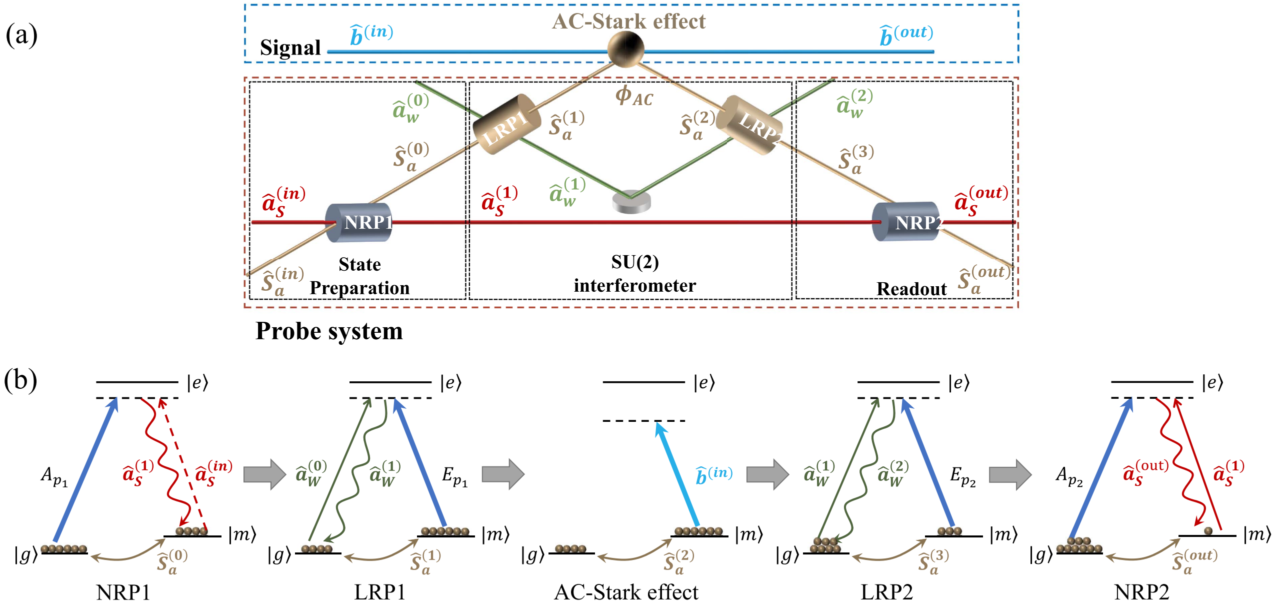

Fig. 1. (a) Schematic of QND measurement of photon number. The probe system consists of an SU(1,1)-SU(2)-concatenated atom–light hybrid interferometer. In the SU(2) interferometer in the middle box, the LRP is utilized to realize the splitting and combination of the atomic spin wave and the optical wave. $\hat{a}_W^{(0)}$ is a coherent state, and $\hat{S}_a^{(0)}$, $\hat{S}_a^{(1)}$, and $\hat{S}_a^{(3)}$ are atomic collective excitations prepared by NRP1, LRP1, and LRP2, respectively. The atomic spin wave $\hat{S}_a^{(1)}$ experiences a phase modulation ϕ_{AC} via the AC-Stark effect by signal light $\hat{b}^{(\mathrm{in})}$ and evolves to $\hat{S}_a^{(2)}$. The generated atomic spin wave $\hat{S}_a^{(3)}$ of the SU(2) interferometer and the optical wave $\hat{a}_S^{(1)}$, which is correlated with $\hat{S}_a^{(0)}$, are combined to realize active correlation output readout via NRP2. LRP, linear Raman process; NRP, nonlinear Raman process. (b) Energy levels of the atom. The lower two energy states $|g\rangle$ and $|m\rangle$ are the hyperfine split ground states. The higher-energy state $|e\rangle$ is the excited state. The strong pump field A_{p_1} (A_{p_2}) and strong read field E_{p_1} (E_{p_2}) couple the transitions $|g\rangle \to |e\rangle$ and $|m\rangle \to |e\rangle$, respectively. $\hat{b}^{(\mathrm{in})}$ is far off resonance with the transition $|m\rangle \to |e\rangle$ by a large detuning.

input operators with three steps: (1) state preparation; (2) SU(2) interferometer, and (3) readout. In the first step, we prepare the initial atomic spin wave $\hat{S}_a^{(0)}$ and a correlated optical wave $\hat{a}_S^{(1)}$ via NRP1. It can be described as

$$\hat{S}_a^{(0)} = G_1 \hat{S}_a^{(\mathrm{in})} + g_1 e^{i\theta_1} \hat{a}_S^{\dagger(\mathrm{in})}, \quad \hat{a}_S^{(1)} = G_1 \hat{a}_S^{(\mathrm{in})} + g_1 e^{i\theta_1} \hat{S}_a^{\dagger(\mathrm{in})}. \tag{5}$$

Next, the beam splitter in an SU(2) interferometer is provided by the LRP, which can split and mix the atomic spin wave and the optical wave coherently for interference. $\hat{a}_W^{(0)}$ is a coherent state, and $\hat{S}_a^{(0)}$ is an atomic collective excitation prepared by NRP1. The relationship between input and output in the SU(2) interferometer is given by

$$\hat{S}_a^{(3)} = t\hat{S}_a^{(0)} + r\hat{a}_W^{(0)}, \quad \hat{a}_W^{(2)} = t\hat{a}_W^{(0)} + r\hat{S}_a^{(0)}, \tag{6}$$

where $t = e^{i\phi/2}\cos(\phi/2)$, $r = ie^{i\phi/2}\sin(\phi/2)$, and ϕ denotes the phase shift.

In the final step, the generated atomic spin wave $\hat{S}_a^{(3)}$ of the SU(2) interferometer and the optical wave $\hat{a}_S^{(1)}$ are combined to realize active correlation output readout via NRP2. It can be expressed as

$$\begin{aligned} \hat{S}_a^{(\mathrm{out})} &= G_2 \hat{S}_a^{(3)} + g_2 e^{i\theta_2} \hat{a}_S^{\dagger(1)}, \\ \hat{a}_S^{(\mathrm{out})} &= G_2 \hat{a}_S^{(1)} + g_2 e^{i\theta_2} \hat{S}_a^{\dagger(3)}. \end{aligned} \tag{7}$$

And thus, the full input–output relation of the actively correlated atom-light hybrid interferometer is

$$\begin{aligned} \hat{a}_S^{(\mathrm{out})} &= A\hat{a}_S^{(\mathrm{in})} + B\hat{S}_a^{\dagger(\mathrm{in})} + C\hat{a}_W^{\dagger(0)}, \\ \hat{S}_a^{(\mathrm{out})} &= D\hat{a}_S^{\dagger(\mathrm{in})} + E\hat{S}_a^{(\mathrm{in})} + F\hat{a}_W^{(0)}, \end{aligned} \tag{8}$$

where

$$\begin{aligned} &A = G_2 G_1 + g_2 g_1 e^{i(\theta_2 - \theta_1)} t^*, B = G_2 g_1 e^{i\theta_1} + G_1 g_2 e^{i\theta_2} t^*, \\ &D = G_1 g_2 e^{i\theta_2} + G_2 g_1 e^{i\theta_1} t, E = g_2 g_1 e^{i(\theta_2 - \theta_1)} + G_2 G_1 t, \\ &C = g_2 e^{i\theta_2} r^*, F = G_2 r. \end{aligned} \tag{9}$$

3. QND MEASUREMENT OF PHOTON NUMBER

This new type interferometer in Section 2 can be used as a probe system for QND measurement. The schematic of QND measurement of a photon number is shown in Fig. 1(a); when the atom system of this new type interferometer is illuminated by the off-resonant signal light $\hat{b}^{(\mathrm{in})}$, the interaction between the atom and signal light $\hat{b}^{(\mathrm{in})}$ will induce an atomic phase shift [51,52]:

$$\phi_{\mathrm{AC}} = \kappa \hat{n}_b, \tag{10}$$

where $\hat{n}_b = \hat{b}^{(\mathrm{in})\dagger}\hat{b}^{(\mathrm{in})}$ is the photon number operator of the signal light, and κ is the AC-Stark coefficient.

In this QND measurement scheme, the photon number of the signal light is the QND observable, while the phase of the signal light is the conjugated observable. The quantum noise induced by the act of measurement is fed into the unmeasured conjugate observable $\phi^{(s)}$ of the signal light, where superscript

(s) denotes the signal light. The uncertainty of these two observables is limited by the Heisenberg relation $\Delta n_b^{(s)} \Delta \phi^{(s)} \geq 1$ [53]. That is, the QND measurement of the observable $n_b^{(s)}$ is accomplished at the expense of an uncertainty increase in its conjugate observable $\phi^{(s)}$. By monitoring the atomic phase shift ϕ_{AC} using this atom-light hybrid interferometer, we can determine the photon number of the signal light without destroying the photons. The phase shift of the atomic spin wave is the readout observable, which can be measured by homodyne detection. Next, we analyze the performance of this scheme as a QND measurement.

A. SNR Analysis

The QND measurement scheme that uses the AC-Stark effect is based on the precision measurement of the photon-induced atomic phase shift; thus, the SNR analysis is helpful to examine the performance of the QND measurement process. Given the homodyne detection, the SNR is defined as

$$R = \frac{\langle \hat{X}_S^{(\mathrm{out})} \rangle^2}{\langle \Delta^2 \hat{X}_S^{(\mathrm{out})} \rangle}, \tag{11}$$

where $\langle \hat{X}_S^{(\mathrm{out})} \rangle$ and $\langle \Delta^2 \hat{X}_S^{(\mathrm{out})} \rangle$ denote the quantum expectation and variance of the amplitude quadrature, respectively. In our scheme, they are given by

$$\begin{aligned} \langle \hat{X}_S^{(\mathrm{out})} \rangle &= \langle \hat{a}_S^{(\mathrm{out})} + \hat{a}_S^{\dagger(\mathrm{out})} \rangle \\ &= g_2 N_\alpha^{1/2} [\cos(\theta_2 - \theta_\alpha - \phi) - \cos(\theta_2 - \theta_\alpha)], \end{aligned} \tag{12}$$

$$\begin{aligned} \langle \Delta^2 \hat{X}_S^{(\mathrm{out})} \rangle = {} & G_2^2 G_1^2 + G_2^2 g_1^2 + g_2^2 (1 - \cos\phi)/2 \\ & + g_2^2 g_1^2 (1 + \cos\phi)/2 + G_1^2 g_2^2 (1 + \cos\phi)/2 \\ & + 2 G_2 G_1 g_2 g_1 \cos(\theta_2 - \theta_1 - \phi) \\ & + 2 G_2 G_1 g_2 g_1 \cos(\theta_2 - \theta_1). \end{aligned} \tag{13}$$

Here $\hat{a}_S^{(\mathrm{in})}$ and $\hat{S}_a^{(\mathrm{in})}$ are in vacuum states, and $\hat{a}_W^{(0)}$ is in a coherent state $|\alpha\rangle$, with $\alpha = N_\alpha^{1/2} e^{i\theta_\alpha}$, where N_α and θ_α are the photon number and initial phase of the coherent state, respectively. The phase shift ϕ includes the phase difference ϕ_0 of the interferometer and the phase difference ϕ_{AC} caused by the AC-Stark effect, with $\phi_{\mathrm{AC}} = \kappa \hat{n}_b$. Our scheme can be thought of as inserting an SU(2) interferometer into one of the arms of the SU(1,1) interferometer. For a balanced SU(1,1) interferometer configuration, two NRPs of equal gain ($g_2 = g_1 = g$) and opposite pump phases ($\theta_1 = 0$, $\theta_2 = \pi$) are arranged in series. NRP1 produces an optical field together with a correlated atomic spin excitation, while NRP2 is shifted in pump phase to exactly reverse the operation of NRP1 and return the optical field and atomic spin excitation back to their original input states. When a phase shift is introduced, the transfer is no longer complete, and thus leads to a change in the output corresponding to the induced phase shift. Here we first consider a balanced case in which the SU(2) interferometer is introduced into a balanced SU(1,1) interferometer. With a small ϕ_{AC} around $\phi_0 = 0$ and $\alpha = i N_\alpha^{1/2}$, assuming the signal light is in a number state $|n\rangle$ with $\hat{n}_b |n\rangle = n_b |n\rangle$ and substituting ϕ_{AC} with $\kappa \hat{n}_b$, the SNR is

$$R \approx g^2 \kappa^2 N_\alpha n_b^2. \tag{14}$$

To have single-photon resolution, we need AC-Stark coefficient $\kappa \sim 1/g N_\alpha^{1/2}$. Compared to the traditional SU(2) interferometer [45], the required coefficient is smaller by a factor of $1/g$. This is due to the method of active correlation output readout for the SU(2) interferometer [54], in which the SNR is greater than for the SU(2) interferometer by a factor of g of NRP.

B. Quality Estimation

In QND measurement, the signal light is coupled to the probe system, and a subsequent readout measurement of the probe output is made to extract the information about the signal light without perturbing it. An ideal QND measurement requires a perfect correlation between the signal and the probe system. In practice, the probe output itself has fluctuation, which leads to a nonideal QND measurement. Thus the quality of the QND measurement scheme is worth studying. In this section, we estimate the quality using the criteria introduced by Holland *et al.* [47], which are

$$C^2_{S^{\mathrm{in}} S^{\mathrm{out}}} = \frac{|\langle S^{\mathrm{in}} S^{\mathrm{out}} \rangle - \langle S^{\mathrm{in}} \rangle \langle S^{\mathrm{out}} \rangle|^2}{\langle \Delta^2 S^{\mathrm{in}} \rangle \langle \Delta^2 S^{\mathrm{out}} \rangle}, \tag{15}$$

$$C^2_{S^{\mathrm{in}} P^{\mathrm{out}}} = \frac{|\langle S^{\mathrm{in}} P^{\mathrm{out}} \rangle - \langle S^{\mathrm{in}} \rangle \langle P^{\mathrm{out}} \rangle|^2}{\langle \Delta^2 S^{\mathrm{in}} \rangle \langle \Delta^2 P^{\mathrm{out}} \rangle}, \tag{16}$$

$$C^2_{S^{\mathrm{out}} P^{\mathrm{out}}} = \frac{|\langle S^{\mathrm{out}} P^{\mathrm{out}} \rangle - \langle S^{\mathrm{out}} \rangle \langle P^{\mathrm{out}} \rangle|^2}{\langle \Delta^2 S^{\mathrm{out}} \rangle \langle \Delta^2 P^{\mathrm{out}} \rangle}, \tag{17}$$

with

$$\begin{aligned} \langle \Delta^2 S^{\mathrm{in}} \rangle &= \langle (S^{\mathrm{in}})^2 \rangle - \langle S^{\mathrm{in}} \rangle^2, \\ \langle \Delta^2 S^{\mathrm{out}} \rangle &= \langle (S^{\mathrm{out}})^2 \rangle - \langle S^{\mathrm{out}} \rangle^2, \\ \langle \Delta^2 P^{\mathrm{in}} \rangle &= \langle (P^{\mathrm{in}})^2 \rangle - \langle P^{\mathrm{in}} \rangle^2, \\ \langle \Delta^2 P^{\mathrm{out}} \rangle &= \langle (P^{\mathrm{out}})^2 \rangle - \langle P^{\mathrm{out}} \rangle^2, \end{aligned} \tag{18}$$

where S^{in} is the input signal incident on the scheme, and P^{out} is the output probe measured by a detector. Here S^{in} is the photon number of the input signal $\hat{N}^{(\mathrm{in})} = \hat{b}^{\dagger(\mathrm{in})} \hat{b}^{(\mathrm{in})}$, and the probe is the amplitude quadrature $\hat{X}_S^{(\mathrm{out})}$. Equation (15) shows how much the probe system degrades the signal of the measured system. Equation (16) shows how good the probe system is as a measurement device. Equation (17) shows how good the probe system is as a state preparation device. For an ideal QND measurement device, the correlation coefficients $C^2_{S^{\mathrm{in}} S^{\mathrm{out}}}$, $C^2_{S^{\mathrm{in}} P^{\mathrm{out}}}$, and $C^2_{S^{\mathrm{out}} P^{\mathrm{out}}}$ are unity. In our paper, the signal light leading to the AC-Stark shift is far off resonance with a large detuning, i.e., the photon number of the measured signal light is not changed before or after measurement. So the first criterion is satisfied, and the second and third criteria become the same: $C^2_{\hat{N}^{(\mathrm{in})} \hat{X}_S^{(\mathrm{out})}} = C^2_{\hat{N}^{(\mathrm{out})} \hat{X}_S^{(\mathrm{out})}}$, that is,

$$C^2 = \frac{|\langle \hat{N}^{(\mathrm{in})} \hat{X}_S^{(\mathrm{out})} \rangle - \langle \hat{N}^{(\mathrm{in})} \rangle \langle \hat{X}_S^{(\mathrm{out})} \rangle|^2}{\langle \Delta^2 \hat{N}^{(\mathrm{in})} \rangle \langle \Delta^2 \hat{X}_S^{(\mathrm{out})} \rangle}. \tag{19}$$

For brevity, we omit the subscript of C. In the previous section, even if we assume the signal light is in a number state, which is the eigenstate of the photon number measurement process ($\hat{n}_b|n\rangle = n_b|n\rangle$), the probe output has fluctuation and does not yield a definite value. Here, for convenience, the signal light is set in a coherent state $|\beta\rangle$ with photon number N_β. We obtain

$$\begin{aligned}\langle \hat{N}^{(\mathrm{in})}\rangle &= N_\beta,\ \Delta^2\hat{N}^{(\mathrm{in})} = N_\beta,\\ \langle \hat{X}_S^{(\mathrm{out})}\rangle &= g_2\kappa N_\alpha^{1/2}N_\beta,\\ \langle \hat{N}^{(\mathrm{in})}\hat{X}_S^{(\mathrm{out})}\rangle &= g_2\kappa N_\alpha^{1/2}N_\beta(N_\beta+1),\\ \langle \Delta^2\hat{X}_S^{(\mathrm{out})}\rangle &= (G_2G_1-g_2g_1)^2+(G_2g_1-G_1g_2)^2\\ &\quad + g_2^2\kappa^2N_\alpha N_\beta + G_1^2g_2^2\kappa^2N_\beta(N_\beta+1)/2. \end{aligned} \tag{20}$$

Substituting Eq. (20) into Eq. (19), the criteria can be written as

$$C^2 = \frac{1}{1+\frac{(G_2G_1-g_2g_1)^2+(G_2g_1-G_1g_2)^2}{g_2^2\kappa^2N_\alpha N_\beta}+\frac{G_1^2(N_\beta+1)}{2N_\alpha}}. \tag{21}$$

As seen in Eq. (21), a perfect correlation $C^2 \approx 1$ can be satisfied under the condition of $g_2^2\kappa^2N_\alpha N_\beta \gg (G_2G_1-g_2g_1)^2 + (G_2g_1-G_1g_2)^2$ and $2N_\alpha \gg G_1^2(N_\beta+1)$. In a balanced case, the condition for a perfect correlation is $g^2\kappa^2N_\alpha N_\beta \gg 1$ and $2N_\alpha \gg G^2(N_\beta+1)$.

C. Optimized *C* in the Presence of Losses

Next, we investigate the effects of losses on the correlation coefficient C in the presence of photon losses and atomic decoherence losses [43].

The loss of the two arms inside the SU(2) interferometer is called internal loss, as shown in Fig. 2(a). The loss at the output of SU(2) and the associated optical field is called external loss, as shown in Fig. 2(b). Two fictitious beam splitters are introduced to mimic the loss of photons into the environment, and then optical waves $\hat{a}_W^{(1)}$ and $\hat{a}_S^{(1)}$ experience losses as

$$\hat{a}_{W,l}^{(1)} = \sqrt{\eta_1}\hat{a}_W^{(1)} + \sqrt{1-\eta_1}\hat{V}_1, \tag{22}$$

$$\hat{a}_{S,l}^{(1)} = \sqrt{\eta_2}\hat{a}_S^{(1)} + \sqrt{1-\eta_2}\hat{V}_2, \tag{23}$$

where subscript l indicates the loss, and η_1 (η_2) and $\hat{V}_1$ ($\hat{V}_2$) represent the transmission rate and vacuum, respectively. The

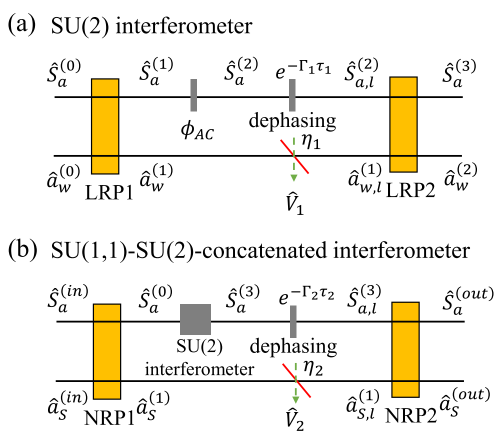

Fig. 2. Lossy interferometer model with (a) internal loss and (b) external loss.

spin waves $\hat{S}_a^{(2)}$ ($\hat{S}_a^{(3)}$) also undergo collisional dephasing $e^{-\Gamma_1\tau_1}$ ($e^{-\Gamma_2\tau_2}$), and then the spin waves are described by

$$\hat{S}_{a,l}^{(2)} = \hat{S}_a^{(2)}e^{-\Gamma_1\tau_1} + \hat{F}_1, \tag{24}$$

$$\hat{S}_{a,l}^{(3)} = \hat{S}_a^{(3)}e^{-\Gamma_2\tau_2} + \hat{F}_2, \tag{25}$$

where $\langle \hat{F}_1\hat{F}_1^\dagger\rangle = 1-e^{-2\Gamma_1\tau_1}$ and $\langle \hat{F}_2\hat{F}_2^\dagger\rangle = 1-e^{-2\Gamma_2\tau_2}$ guarantee the consistency of the operator properties of $\hat{S}_{a,l}^{(2)}$ and $\hat{S}_{a,l}^{(3)}$, respectively. The input–output relation for the loss case of $\hat{a}_S^{(\mathrm{out})}$ becomes

$$\begin{aligned}\hat{a}_{S,l}^{(\mathrm{out})} &= \hat{a}_S^{(\mathrm{in})}\mathcal{A} + \hat{S}_a^{\dagger(\mathrm{in})}\mathcal{B} + \hat{a}_W^{\dagger(0)}\mathcal{C} + \hat{V}_1^\dagger\mathcal{D}\\ &\quad + \hat{V}_2\mathcal{E} + \hat{F}_1^\dagger\mathcal{F} + \hat{F}_2^\dagger\mathcal{G}, \end{aligned} \tag{26}$$

where

$$\begin{aligned}\mathcal{A} &= [\sqrt{\eta_2}G_2G_1 + g_2g_1e^{i(\theta_2-\theta_1)}(e^{-\Gamma_1\tau_1}e^{-i\phi} + \sqrt{\eta_1})e^{-\Gamma_2\tau_2}/2],\\ \mathcal{B} &= [\sqrt{\eta_2}G_2g_1e^{i\theta_1} + G_1g_2e^{i\theta_2}(e^{-\Gamma_1\tau_1}e^{-i\phi} + \sqrt{\eta_1})e^{-\Gamma_2\tau_2}/2],\\ \mathcal{C} &= g_2e^{i\theta_2}(e^{-\Gamma_1\tau_1}e^{-i\phi} - \sqrt{\eta_1})e^{-\Gamma_2\tau_2}/2,\\ \mathcal{D} &= -g_2e^{i\theta_2}\sqrt{1-\eta_1}e^{-\Gamma_2\tau_2}/\sqrt{2},\\ \mathcal{E} &= G_2\sqrt{1-\eta_2},\\ \mathcal{F} &= g_2e^{i\theta_2}e^{-\Gamma_2\tau_2}/\sqrt{2},\\ \mathcal{G} &= g_2e^{i\theta_2}. \end{aligned} \tag{27}$$

We study the effect of losses under the condition of $\theta_1 = 0$, $\theta_2 = \pi$, $\theta_\alpha = \pi/2$, and $\phi_0 = 0$, with a small ϕ_{AC} around ϕ_0. Considering losses, the terms of $\langle \hat{X}_S^{(\mathrm{out})}\rangle_l$, $\langle \hat{N}^{(\mathrm{in})}\hat{X}_S^{(\mathrm{out})}\rangle_l$, and $\langle \Delta^2\hat{X}_S^{(\mathrm{out})}\rangle_l$ in Eq. (20) are given by

$$\langle \hat{X}_S^{(\mathrm{out})}\rangle_l = g_2e^{-\Gamma_1\tau_1}e^{-\Gamma_2\tau_2}\kappa N_\alpha^{1/2}N_\beta, \tag{28}$$

$$\langle \hat{N}^{(\mathrm{in})}\hat{X}_S^{(\mathrm{out})}\rangle_l = g_2e^{-\Gamma_1\tau_1}e^{-\Gamma_2\tau_2}\kappa N_\alpha^{1/2}N_\beta(N_\beta+1), \tag{29}$$

and

$$\begin{aligned}&\langle \Delta^2\hat{X}_S^{(\mathrm{out})}\rangle_l\\ &\quad = (\sqrt{\eta_2}G_2G_1 - g_2g_1e^{-\Gamma_1\tau_1}e^{-\Gamma_2\tau_2}/2 - g_2g_1e^{-\Gamma_2\tau_2}\sqrt{\eta_1}/2)^2\\ &\quad + (\sqrt{\eta_2}G_2g_1 - G_2g_2e^{-\Gamma_1\tau_1}e^{-\Gamma_2\tau_2}/2 - G_1g_2e^{-\Gamma_2\tau_2}\sqrt{\eta_1}/2)^2\\ &\quad + g_2^2[(1-e^{-2\Gamma_1\tau_1})e^{-2\Gamma_2\tau_2}/2 + (1-e^{-2\Gamma_2\tau_2})]\\ &\quad + g_2^2(2g_1^2+1)\kappa^2N_\beta(N_\beta+1)e^{-2\Gamma_1\tau_1}e^{-2\Gamma_2\tau_2}/4\\ &\quad + g_2^2\kappa^2N_\beta[N_\alpha + (N_\beta+1)/4]e^{-2\Gamma_1\tau_1}e^{-2\Gamma_2\tau_2}\\ &\quad + (g_2e^{-\Gamma_2\tau_2}\sqrt{\eta_1}/2 - g_2e^{-\Gamma_1\tau_1}e^{-\Gamma_2\tau_2}/2)^2\\ &\quad + g_2^2(1-\eta_1)e^{-2\Gamma_2\tau_2}/2 + G_2^2(1-\eta_2), \end{aligned} \tag{30}$$

and then the QND measurement criterion for the loss case can be obtained according to Eq. (19).

In our scheme, the atomic spin wave stays in the atomic ensemble, while the optical field travels out of the atomic ensemble. Here, within the coherence time, the atomic collisional dephasing loss $\Gamma_1\tau_1(\Gamma_2\tau_2)$ is small, and then we set $e^{-\Gamma_1\tau_1} = e^{-\Gamma_2\tau_2} = 0.9$. The correlation coefficient C as a function of η_1 and η_2 in the balanced case is shown in Fig. 3. It is shown that the reduction in the correlation coefficient C increases as the loss increases, and that our scheme is more tolerant with the

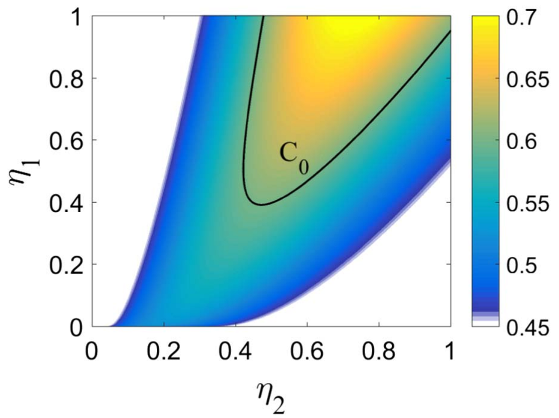

Fig. 3. Correlation coefficient C as a function of η_1 and η_2, where $e^{-\Gamma_1\tau_1} = e^{-\Gamma_2\tau_2} = 0.9$, $\kappa = 10^{-10}$, $g_1 = g_2 = 3$, $N_\alpha = 10^{12}$, and $N_\beta = 10^8$. The correlation coefficient in the area of upper right corner and within the C_0 lines can be kept above 0.6.

internal photon loss η_1 compared to the photon loss outside the SU(2) interferometer η_2. The reason behind the phenomenon is that a large external photon loss affects the quantum correlation between the light wave and atomic spin wave, which destroys the active correlation output readout.

In the unbalanced case ($g_1 \neq g_2$), we can adjust the gain ratio g_2/g_1 of the beam recombination process to reduce the reduction in correlation coefficient. The black line in Fig. 3 is labeled as C_0, as a benchmark for comparison before and after optimization; here we set $C_0 = 0.6$. The correlation coefficient in the area of the upper right corner and within the C_0 lines can be kept above 0.6. After optimizing g_2, the correlation coefficient as a function of η_1 and η_2 can also be obtained, where the line with C equal to 0.6 is denoted as C_1. The contour lines of optimized g_2/g_1 as a function of η_1 and η_2 are shown in Fig. 4, where the position of C_0 (before optimization) and C_1 (after optimization) in the contour figure of the correlation coefficient versus transmission rates has changed. It is demonstrated that for a given g_1 by optimizing g_2/g_1, the small area between C_0 and C_1 can still stay above 0.6. That is, within a certain loss range, C can continue to beat the criteria (such as C equal to 0.6) after optimizing g_2/g_1. The newly added area after optimization is divided into two parts: (1) ratio g_2/g_1 within the very small area above is less than one, and (2) ratio g_2/g_1 needs to be greater than one.

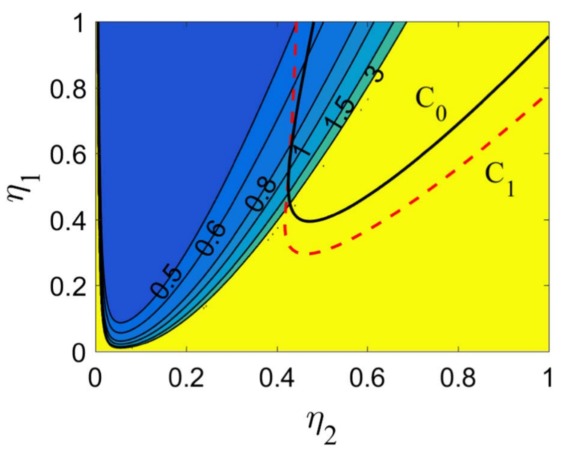

Fig. 4. Contour line of optimized g_2/g_1 as a function of η_1 and η_2, with $e^{-\Gamma_1\tau_1} = e^{-\Gamma_2\tau_2} = 0.9$, where $\kappa = 10^{-10}$, $g_1 = 3$, $N_\alpha = 10^{12}$, and $N_\beta = 10^8$. The correlation coefficient in the area of upper right corner and within the line C_0 (before optimization) or C_1 (after optimization) can be kept above 0.6.

4. DISCUSSION AND CONCLUSION

In our scheme, the spin wave prepared by the first NRP participates in the subsequent LRP and NRP, and additional operations are required within the coherence time of the spin wave compared to previous experimental works on atom-light interferometers [40,41]; therefore, the pulse width and intensity of the pump field $A_{p_1}(A_{p_2})$ and the read field $E_{p_1}(E_{p_2})$ should be properly arranged. Experimental consideration of the implementation of the scheme may be performed with a rubidium atomic vapor in a cell. The energy levels of the Rb atom are shown in Fig. 1(b), where states $|g\rangle$ and $|m\rangle$ are the two ground states $|5^2S_{1/2}, F = 1,2\rangle$ from hyperfine splitting, and $|e\rangle$ is the excited state $|5^2P_{1/2}, F = 2\rangle$. The signal field is far resonance with the transition $|5^2S_{1/2}, F = 2\rangle \rightarrow |5^2P_{1/2}, F = 2\rangle$ by 2–4 GHz detuning [40]. The interaction between the atom and signal light will induce an atomic phase shift that is proportional to the photon number of the signal field. With a detuning 2 GHz and photon number of signal light $N_\beta = 10^8$, the AC-Stark coupling coefficient κ is $\sim 10^{-10}$ rad per photon [45]. With a gain $g^2 = 10$ obtained by turning the pumping field intensity, to realize a perfect correlation, the theoretical requirement $N_\alpha N_\beta \gg (1/g\kappa)^2 = 10^{19}$ and $N_\alpha \gg 5.5N_\beta$ should be satisfied. Since given $N_\beta = 10^8$, we choose $N_\alpha = 10^{12}$. In the calculations, the photon numbers are much smaller than the number of atoms in the interaction region. Thus, the density of the atomic sample is 10^{13}–10^{14} cm^{-3} by controlling the cell temperature. The signal light is turned on after the first linear Raman splitting process and turned off right before the second linear Raman mixing process. The pulse width of signal light should be short, and in this way, it will not affect the LRP for splitting and mixing the atomic and optical waves. Here we set the pulse width of signal field $\sim$100 ns. To realize $N_\beta = 10^8$, the power of signal light is $\sim$0.25 mW for wavelength 0.795 μm with coherent time 100 ns. The mean photon number $N_\alpha = 10^{12}$ of $\hat{a}_W^{(0)}$ field is given with $\sim$2.5 mW of coherent time 100 μs for wavelength 0.795 μm. The requirement for the number of photons N_α and N_β can be met and be feasible in the experiment.

In conclusion, we have proposed an SU(1,1)-SU(2)-concatenated atom-light hybrid interferometer and used it for QND measurement of photon numbers via the AC-Stark effect. In the scheme, the atomic spin wave of the SU(2) interferometer is prepared via an NRP, and the output is detected with the method of active correlation output readout via another NRP. Benefiting from that, the SNR in the balanced case is improved by a factor of g compared to the traditional SU(2) interferometer. The condition for a perfect correlation is given. The measurement quality is reduced in the presence of losses. We can adjust the gain parameter of the NRP in the readout stage to reduce the impact of losses. Moreover, the scheme is a multiarm interferometer, and it provides an option for the simultaneous estimation of more than two parameters with a wide range of applications, such as phase imaging [55], quantum sensing networks [56], and detection of vector fields [57].

Funding. National Key Research and Development Program of China (2016YFA0302001); National Natural Science Foundation of China (11974111, 11874152, 91536114, 11574086, 11974116, 11654005); Shanghai Rising-Star Program (16QA1401600); Innovation Program of Shanghai Municipal Education Commission (202101070008E00099); Shanghai Talent Program; Chinese National Youth Talent Support Program; Fundamental Research Funds for the Central Universities.

Disclosures. The authors declare no conflicts of interest.

Data Availability. Data underlying the results presented in this paper are not publicly available at this time but may be obtained from the authors upon reasonable request.

REFERENCES

1. C. M. Caves, K. S. Thorne, R. W. P. Drever, V. D. Sandberg, and M. Zimmermann, "On the measurement of a weak classical force coupled to a quantum-mechanical oscillator. I. Issues of principle," Rev. Mod. Phys. **52**, 341–392 (1980).
2. M. F. Bocko and R. Onofrio, "On the measurement of a weak classical force coupled to a harmonic oscillator: experimental progress," Rev. Mod. Phys. **68**, 755–799 (1996).
3. V. B. Braginsky and F. Y. Khalili, "Quantum nondemolition measurements: the route from toys to tools," Rev. Mod. Phys. **68**, 1–11 (1996).
4. F. Lecocq, J. B. Clark, R. W. Simmonds, J. Aumentado, and J. D. Teufel, "Quantum non-demolition measurement of a nonclassical state of a massive object," Phys. Rev. X **5**, 041037 (2015).
5. M. Rossi, D. Mason, J. Chen, Y. Tsaturyan, and A. Schliesser, "Measurement-based quantum control of mechanical motion," Nature **563**, 53–58 (2018).
6. D. B. Hume, T. Rosenband, and D. J. Wineland, "High-fidelity adaptive qubit detection through repetitive quantum non-demolition measurements," Phys. Rev. Lett. **99**, 120502 (2007).
7. F. Wolf, Y. Wan, J. C. Heip, F. Gebert, C. Shi, and P. O. Schmidt, "Non-destructive state detection for quantum logic spectroscopy of molecular ions," Nature **530**, 457–460 (2016).
8. M. Raha, S. Chen, C. M. Phenicie, S. Ourari, A. M. Dibos, and J. D. Thompson, "Optical quantum non-demolition measurement of a single rare earth ion qubit," Nat. Commun. **11**, 1605 (2020).
9. X. Xue, B. D'Anjou, T. F. Watson, D. R. Ward, D. E. Savage, M. G. Lagally, M. Friesen, S. N. Coppersmith, M. A. Eriksson, W. A. Coish, and L. M. K. Vandersypen, "Repetitive quantum non-demolition measurement and soft decoding of a silicon spin qubit," Phys. Rev. X **10**, 021006 (2020).
10. S. Hacohen-Gourgy, L. S. Martin, E. Flurin, V. V. Ramasesh, K. B. Whaley, and I. Siddiqi, "Quantum dynamics of simultaneously measured non-commuting observables," Nature **538**, 491–494 (2016).
11. U. Vool, S. Shankar, S. O. Mundhada, N. Ofek, A. Narla, K. Sliwa, E. Zalys-Geller, Y. Liu, L. Frunzio, R. J. Schoelkopf, S. M. Girvin, and M. H. Devoret, "Continuous quantum non-demolition measurement of the transverse component of a qubit," Phys. Rev. Lett. **117**, 133601 (2016).
12. P. Grangier, J. A. Levenson, and J.-P. Poizat, "Quantum non-demolition measurements in optics," Nature **396**, 537–542 (1998).
13. A. Reiserer, S. Ritter, and G. Rempe, "Non-destructive detection of an optical photon," Science **342**, 1349–1351 (2013).
14. S. Kono, K. Koshino, Y. Tabuchi, A. Noguchi, and Y. Nakamura, "Quantum non-demolition detection of an itinerant microwave photon," Nat. Phys. **14**, 546–549 (2018).
15. N. Imoto, H. A. Haus, and Y. Yamamoto, "Quantum nondemolition measurement of the photon number via the optical Kerr effect," Phys. Rev. A **32**, 2287–2292 (1985).
16. M. J. Holland, D. F. Walls, and P. Zoller, "Quantum nondemolition measurements of photon number by atomic beam deflection," Phys. Rev. Lett. **67**, 1716–1719 (1991).
17. S. R. Friberg, S. Machida, and Y. Yamamoto, "Quantum-nondemolition measurement of the photon number of an optical soliton," Phys. Rev. Lett. **69**, 3165–3168 (1992).
18. K. Jacobs, P. Tombesi, M. J. Collett, and D. F. Walls, "Quantum-nondemolition measurement of photon number using radiation pressure," Phys. Rev. A **49**, 1961–1966 (1994).
19. Y. Sakai, R. J. Hawkins, and S. R. Friberg, "Soliton-collision interferometer for the quantum nondemolition measurement of photon number: numerical results," Opt. Lett. **15**, 239–241 (1990).
20. P. Kok, H. Lee, and J. P. Dowling, "Single-photon quantum-nondemolition detectors constructed with linear optics and projective measurements," Phys. Rev. A **66**, 063814 (2002).
21. C. C. Gerry and T. Bui, "Quantum non-demolition measurement of photon number using weak nonlinearities," Phys. Lett. A **372**, 7101–7104 (2008).
22. W. J. Munro, K. Nemoto, R. G. Beausoleil, and T. P. Spiller, "High-efficiency quantum-nondemolition single-photonnumber-resolving detector," Phys. Rev. A **71**, 033819 (2005).
23. G. Nogues, A. Rauschenbeutel, S. Osnaghi, M. Brune, J. M. Raimond, and S. Haroche, "Seeing a single photon without destroying it," Nature **400**, 239–242 (1999).
24. Y. F. Xiao, S. K. Ozdemir, V. Gaddam, C. H. Dong, N. Imoto, and L. Yang, "Quantum nondemolition measurement of photon number via optical Kerr effect in an ultra-high-Q microtoroid cavity," Opt. Express **16**, 21462–21475 (2008).
25. M. Ludwig, A. H. Safavi-Naeini, O. Painter, and F. Marquardt, "Enhanced quantum nonlinearities in a two-mode optomechanical system," Phys. Rev. Lett. **109**, 063601 (2012).
26. D. Malz and J. I. Cirac, "Nondestructive photon counting in waveguide QED," Phys. Rev. Res. **2**, 033091 (2020).
27. J. Liu, H. T. Chen, and D. Segal, "Quantum nondemolition photon counting with a hybrid electromechanical probe," Phys. Rev. A **102**, 061501 (2020).
28. C. M. Caves, "Quantum-mechanical noise in an interferometer," Phys. Rev. D **23**, 1693–1708 (1981).
29. B. Yurke, S. L. McCall, and J. R. Klauder, "SU(2) and SU(1,1) interferometers," Phys. Rev. A **33**, 4033–4054 (1986).
30. L. Pezzé and A. Smerzi, "Mach-Zehnder interferometry at the Heisenberg limit with coherent and squeezed-vacuum light," Phys. Rev. Lett. **100**, 073601 (2008).
31. J. P. Dowling, "Quantum optical metrology-the lowdown on high-N00N states," Contemp. Phys. **49**, 125–143 (2008).
32. F. Hudelist, J. Kong, C. Liu, J. Jing, Z. Y. Ou, and W. Zhang, "Quantum metrology with parametric amplifier-based photon correlation interferometers," Nat. Commun. **5**, 3049 (2014).
33. D. Li, B. T. Gard, Y. Gao, C.-H. Yuan, W. Zhang, H. Lee, and J. P. Dowling, "Phase sensitivity at the Heisenberg limit in an SU(1,1) interferometer via parity detection," Phys. Rev. A **94**, 063840 (2016).
34. B. E. Anderson, P. Gupta, B. L. Schmittberger, T. Horrom, C. Hermann-Avigliano, K. M. Jones, and P. D. Lett, "Phase sensing beyond the standard quantum limit with a variation on the SU(1,1) interferometer," Optica **4**, 752–756 (2017).
35. M. Manceau, G. Leuchs, F. Khalili, and M. Chekhova, "Detection loss tolerant supersensitive phase measurement with an SU(1,1) interferometer," Phys. Rev. Lett. **119**, 223604 (2017).
36. W. Du, J. Kong, G. Bao, P. Yang, J. Jia, S. Ming, C.-H. Yuan, J. F. Chen, Z. Y. Ou, M. W. Mitchell, and W. Zhang, "SU(2)-in-SU(1,1) nested interferometer for high sensitivity, loss-tolerant quantum metrology," Phys. Rev. Lett. **128**, 033601 (2022).
37. K. Zheng, M. Mi, B. Wang, L. Xu, L. Hu, S. Liu, Y. Lou, J. Jing, and L. Zhang, "Quantum-enhanced stochastic phase estimation with the SU(1,1) interferometer," Photon. Res. **8**, 1653–1661 (2020).

38. J. Jacobson, G. Björk, and Y. Yamamoto, "Quantum limit for the atom-light interferometer," Appl. Phys. B **60**, 187–191 (1995).
39. G. Campbell, M. Hosseini, B. M. Sparkes, P. K. Lam, and B. C. Buchler, "Time-and frequency-domain polariton interference," New J. Phys. **14**, 033022 (2012).
40. C. Qiu, S. Chen, L. Q. Chen, B. Chen, J. Guo, Z. Y. Ou, and W. Zhang, "Atom-light superposition oscillation and Ramsey-like atom-light interferometer," Optica **3**, 775–780 (2016).
41. B. Chen, C. Qiu, S. Chen, J. Guo, L. Q. Chen, Z. Y. Ou, and W. Zhang, "Atom-light hybrid interferometer," Phys. Rev. Lett. **115**, 043602 (2015).
42. H.-M. Ma, D. Li, C.-H. Yuan, L. Q. Chen, Z. Y. Ou, and W. Zhang, "SU (1,1)-type light-atom-correlated interferometer," Phys. Rev. A **92**, 023847 (2015).
43. Z.-D. Chen, C.-H. Yuan, H.-M. Ma, D. Li, L. Q. Chen, Z. Y. Ou, and W. Zhang, "Effects of losses in the atom-light hybrid SU(1,1) interferometer," Opt. Express **24**, 17766–17778 (2016).
44. S. S. Szigeti, R. J. Lewis-Swan, and S. A. Haine, "Pumped-up SU(1,1) interferometry," Phys. Rev. Lett. **118**, 150401 (2017).
45. S. Y. Chen, L. Q. Chen, Z. Y. Ou, and W. Zhang, "Quantum non-demolition measurement of photon number with atom-light interferometers," Opt. Express **25**, 31827–31839 (2017).
46. D. H. Fan, S. Y. Chen, Z. F. Yu, K. Zhang, and L. Q. Chen, "Quality estimation of non-demolition measurement with lossy atom-light hybrid interferometers," Opt. Express **28**, 9875–9884 (2020).
47. M. J. Holland, M. J. Collett, D. F. Walls, and M. D. Levenson, "Nonideal quantum nondemolition measurements," Phys. Rev. A **42**, 2995–3005 (1990).
48. M. Dabrowski, R. Chrapkiewicz, and W. Wasilewski, "Hamiltonian design in readout from room-temperature Raman atomic memory," Opt. Express **22**, 26076–26091 (2014).
49. J. Nunn, J. H. D. Munns, S. Thomas, K. T. Kaczmarek, C. Qiu, A. Feizpour, E. Poem, B. Brecht, D. J. Saunders, P. M. Ledingham, D. V. Reddy, M. G. Raymer, and I. A. Walmsley, "Theory of noise suppression in Λ-type quantum memories by means of a cavity," Phys. Rev. A **96**, 012338 (2017).
50. S. E. Thomas, T. M. Hird, J. H. D. Munns, B. Brecht, and D. J. Saunders, "Raman quantum memory with built-in suppression of four-wave-mixing noise," Phys. Rev. A **100**, 033801 (2019).
51. S. H. Autler and C. H. Townes, "Stark effect in rapidly varying fields," Phys. Rev. **100**, 703–722 (1955).
52. K. Hammerer, A. S. Sørensen, and E. S. Polzik, "Quantum interface between light and atomic ensembles," Rev. Mod. Phys. **82**, 1041–1093 (2010).
53. W. Heitler, *The Quantum Theory of Radiation* (Oxford University, 1954).
54. G.-F. Jiao, K. Zhang, L. Q. Chen, W. Zhang, and C.-H. Yuan, "Nonlinear phase estimation enhanced by an actively correlated Mach-Zehnder interferometer," Phys. Rev. A **102**, 033520 (2020).
55. M. Tsang, "Quantum imaging beyond the diffraction limit by optical centroid measurements," Phys. Rev. Lett. **102**, 253601 (2009).
56. T. J. Proctor, P. A. Knott, and J. A. Dunningham, "Multiparameter estimation in networked quantum sensors," Phys. Rev. Lett. **120**, 080501 (2018).
57. T. Baumgratz and A. Datta, "Quantum enhanced estimation of a multidimensional field," Phys. Rev. Lett. **116**, 030801 (2016).